frontiers | Frontiers in Earth Science

TYPE Original Research
PUBLISHED 13 September 2022
DOI 10.3389/feart.2022.978982

OPEN ACCESS

EDITED BY
Dadong Liu,
China University of Petroleum, Beijing, China

REVIEWED BY
Lei Chen,
Southwest Petroleum University, China
Wei Yang,
China University of Petroleum, Beijing, China

*CORRESPONDENCE
Zetang Wang,
wangzetang@cumt.edu.cn
Wenli Zhang,
649069716@qq.com

SPECIALTY SECTION
This article was submitted to Structural Geology and Tectonics, a section of the journal Frontiers in Earth Science

RECEIVED 27 June 2022
ACCEPTED 18 August 2022
PUBLISHED 13 September 2022

CITATION
Yu R, Wang Z, Liu C, Zhang W, Zhu Y, Tang M and Che Q (2022), Microstructure and heterogeneity of coal-bearing organic shale in the southeast Ordos Basin, China: Implications for shale gas storage. *Front. Earth Sci.* 10:978982. doi: 10.3389/feart.2022.978982

Microstructure and heterogeneity of coal-bearing organic shale in the southeast Ordos Basin, China: Implications for shale gas storage

Rui Yu[1], Zetang Wang[2]*, Cheng Liu[3], Wenli Zhang[4]*, Yuxuan Zhu[2], Mengmeng Tang[2] and Qianjin Che[2]

[1]School of Mines, China University of Mining and Technology, Xuzhou, Jiangsu, China, [2]School of Resources and Earth Sciences, China University of Mining and Technology, Xuzhou, Jiangsu, China, [3]Key Laboratory of Unconventional Exploration and Development, CNOOC Energy Development Co, LTD, Tianjin, China, [4]School of Management, Xi'an University of Science and Technology, Xi'an, Shaanxi, China

In recent years, the eastern margin of Ordos Basin has attracted much attention as a key base for unconventional natural gas exploration. The pore-fracture structure is an important physical property of shale and provides places and channels for methane storage and migration. In this study, an integrated method of X-ray diffraction, total organic carbon (TOC), vitrinite reflectance (Ro), scanning electron microscopy (SEM), and low-temperature N_2 adsorption was performed to reveal the microstructure and heterogeneity of coal-bearing organic shale in the southeast Ordos Basin. The result indicated that the studied shale belongs to the category of organic-rich shale with an average TOC content of 8.1% and reaches the dry gas stage with a mean Ro value of 2.41%. Hysteresis loop suggests the shapes of pore structure in shale samples are dominated by inkbottle, cylindrical pores or parallel-plate. A positive correlation between kaolinite and pore surface area indicates that kaolinite contributes greatly to micropores with a large specific surface area. Intense hydrocarbon generation promotes gas to escape from organic components' surfaces, thereby increasing the pore volume. Coal-bearing shales with high brittleness may contain more natural microfractures, increasing specific surface area and pore volume. The bocking effect of minerals in microfractures may reduce pore connectivity and connectivity and enhance shale heterogeneity. The pore volume and specific surface area of coal-bearing shale are closely related to the fractal dimensions. The high complexity of the shale microstructure may lead to the formation of more micropores, resulting in a decrease in the average pore size. Besides, organic and clay-hosted pores in coal-bearing shale with high maturity may well be the main storage space for methane, but the methane is mainly stored in organic pores in marine shale.

KEYWORDS

Ordos Basin, coal-bearing shale, pore structure, heterogeneity, shale gas

Introduction

Due to the exhaustion of fossil energy and the deterioration of environment, the exploitation and utilization of coal measures co-associated resources have attracted great attention of coal geologists and energy enterprises in recent years (Hamawand et al., 2013; Zou et al., 2019; Wang et al., 2020; Li et al., 2022a). Coal and its associated resources are mainly composed of solid and fluid resources. Coal-bearing unconventional natural gas is low-carbon clean energy with extensive distribution and outstanding resource potential (Uysal et al., 2000; Dai et al., 2012; Huang et al., 2016; Yu et al., 2022). Therefore, it is of great practical significance to develop unconventional gas resources in coal to supply fossil energy and improve the environment. The two kinds of natural gas occurring in coal measures are mainly composed of coalbed methane and shale gas, and the latter is primarily distributed in organic-rich shale reservoirs (Jarvie et al., 2007; Ross and Bustin, 2009; Hao et al., 2013). Organic shale is a heterogeneous material composed of organic matter and mineral components, and methane molecules exist in shale's microscopic pore structure in free and adsorbed states (Bowker, 2007; Heller and Zoback, 2014). The shale porosity and the nature of pore-fracture connections are the key factors determining the shale gas seepage and migration (McGlade et al., 2013). Although the pore size of the shale matrix is very small, the large specific surface area of the pores is conducive to methane adsorption. Under suitable pressure and fracture conditions, the pores can promote the migration of shale (Shan et al., 2015). Meanwhile, Shale has a heterogeneous structure and composition, mainly manifested in the difference between mineral composition and organic structure (Klaver et al., 2015; Tang et al., 2015; Yang et al., 2017). These heterogeneities determine the pore networks and connectivity of the pore-fracture system in the gas shale reservoir. Therefore, understanding the microstructure and heterogeneity of coal-bearing shale plays an important role in revealing the occurrence of methane.

Recently, a lot of substantial progress has been made in the characterization and analysis of the microstructure of organic shale and coal reservoirs (Valenza et al., 2013; Li et al., 2015; Saif et al., 2017; Yang et al., 2018; Zhu et al., 2019; Yang et al., 2020; Arif et al., 2021). On the one hand, the characterization of reservoir microstructure by fluid injection experiment is recognized as a reliable method to reveal pore structure parameters quantitatively. On the other hand, observing pore types and distribution at the micro/nanoscale by electron microscope is a key technique for qualitative characterization of shale microstructure. Loucks et al. (2009) suggested that the volume and distribution of organic matter and its relationship with pore volume and permeability are helpful to understand the petrophysical properties of mudstone better. Curtis et al. (2012) used a combined focused ion beam and scanning electron microscopy to study the evolution model of secondary organic pores in the Woodford Shale with different degrees of thermal maturity. Tang et al. (2015) studied the effect of material composition on the pore structure of marine shale with high maturity, indicating that the high organic matter content in marine shale will enhance the heterogeneity of the pore system. Yu et al. (2019) stated the contribution of the molecular structure of clay minerals and organic matter to microscopic pores in coal-bearing shale. Liu et al. (2018) used an NMR fluid typing method to build a classification of pore size in shale reservoirs. Kuila et al. (2014) indicated that porosity in clay is the fundamental contribution of mudstone nanostructure, and no open nanoscale porosity existed in the immature mudstone. Studied the effect of lithofacies on the nanopore structure of marine shale, suggesting that Organic matter is likely to be the main contributor to nanopores rather than clay minerals. In addition to the above studies, there are still plenty of petroleum geologists who have done a lot of work on the microstructure of organic shale (Clarkson et al., 2012a; Pan et al., 2017; Gao et al., 2020; Garum et al., 2020). However, some controversies related to the origin and main influencing factors of pores in shale still exist in petroleum geology.

As the largest superimposed basin in China, Ordos Basin has long been considered a multi-energy basin with abundant fossil energy and mineral resources. A set of upper Paleozoic coal-bearing shales in the southeast Ordos Basin is widely considered a potential area for shale gas exploration and development (Li et al., 2022b; Zhang et al., 2022). The coal-bearing shale gas resources of the Shanxi-Taiyuan Formation are in the range of 2800–3200*10^8 m^3 in the Daning-Jixian block, southeastern Ordos Basin (Zeng et al., 2022). Therefore, it is of great application value to study the microstructure of coal-bearing shale reservoir and its shale gas enrichment in this area. Given this, in this study, we first clarify the material composition of coal-bearing shales from the Shanxi Formation in southeast Ordos Basin using X-ray diffraction (XRD), total organic carbon content (TOC), and vitrinite reflectance (Ro). Then, we characterize the pore structures of shale samples using scanning electron microscopy (SEM), low-temperature N_2 adsorption, and fractal technology. Finally, we discuss the influences of shale material composition on pore type, size and distribution and their implications for methane storage.

Samples and methods

Samples

In this work, a total of 10 coal-bearing shale samples were obtained from a shale gas well in the Daning-Jixian block, southeast Ordos Basin (Figure 1A). The burial depth of these samples ranges from 2118 m to 2209 m, and this depth interval is the main

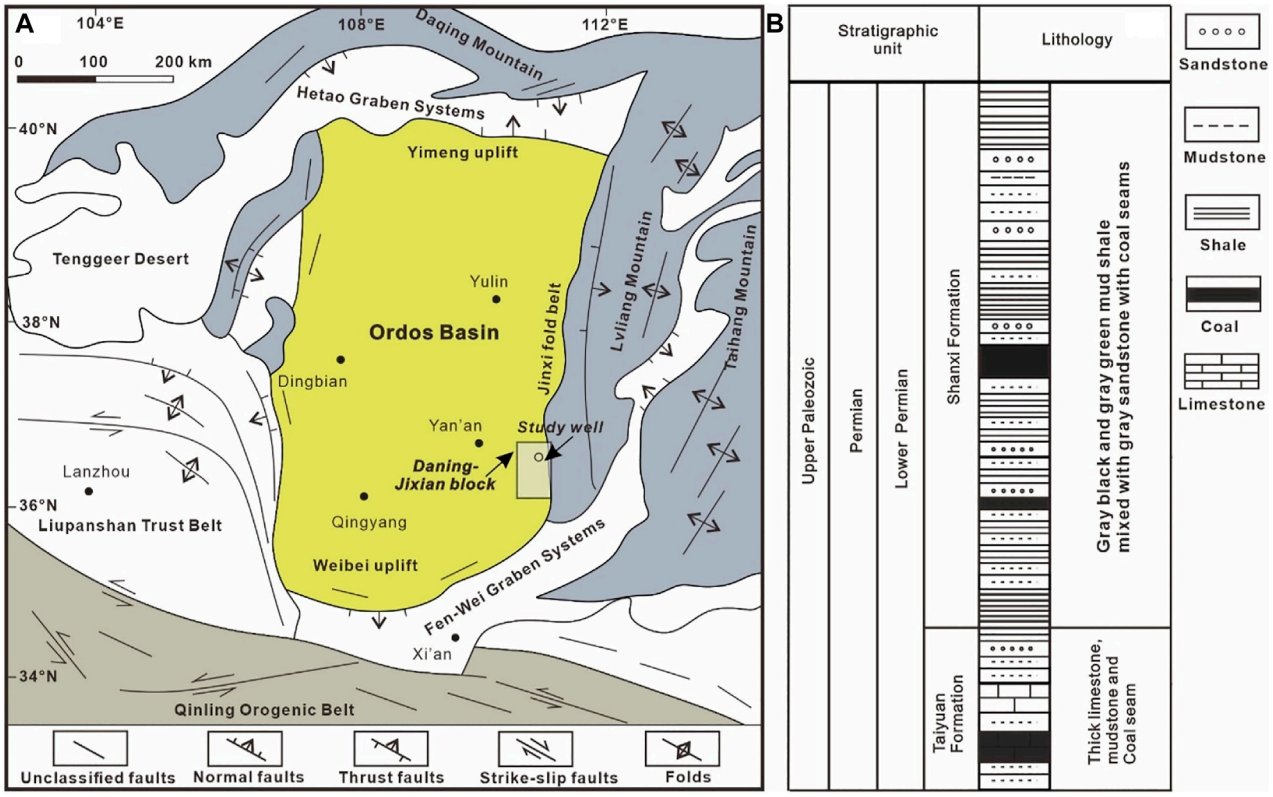

FIGURE 1
Geological map **(A)**, after Ju et al. (2021) and stratigraphic information **(B)** of the southeast Ordos Basin.

TABLE 1 Geological information and major mineral composition of shale samples.

Samples	Depth (m)	TOC (wt%)	Quartz (%)	Clay (%)	Feldspar (%)	Calcite (%)	Dolomite (%)	Siderite (%)	Pyrite (%)	Anatase (%)
SY1	2118	0.80	34.9	57.8	4.4	0.0	0.0	2.9	0.0	0.0
SY2	2127	5.40	29.4	58.3	2.2	0.0	0.0	2.8	5.0	2.4
SY3	2128	5.00	28.0	62.0	1.0	0.0	0.0	2.7	6.2	0.0
SY4	2134	0.10	58.6	23.4	6.5	0.0	10.6	0.8	0.0	0.0
SY5	2146	36.70	17.6	32.2	0.4	3.5	18.3	1.3	25.1	1.7
SY6	2152	1.70	38.8	48.8	7.0	0.0	2.4	3.1	0.0	0.0
SY7	2165	9.40	48.1	45.8	1.3	0.0	0.0	0.0	3.3	1.5
SY8	2166	10.80	43.9	44.3	1.0	0.0	4.1	0.0	5.2	1.5
SY9	2168	8.30	41.3	48.8	0.9	0.0	0.0	0.0	7.4	1.5
SY10	2209	2.70	65.1	28.6	3.7	0.0	0.0	1.1	0.0	1.5

concentration horizon of coal-bearing shale. All samples belong to the Lower Permian Shanxi Formation of late Paleozoic, representing potential source rocks consisting of dispersed organic matters during the sedimentary period of coal measures (Figure 1B). All fresh samples are sealed and stored in airtight bags to prevent weathering before the experiment. The samples were performed on a comprehensive mineralogical and petrophysical testing method, including XRD experiment, TOC analysis, Ro measurement, SEM

test, and N_2 adsorption. The detailed geological information of coal-bearing shale samples is listed in Table 1.

Materials and methods

Quantitative whole rock analysis was applied to reveal the mineral composition of the shale samples, which was performed on X-ray diffraction based on the Chinese Oil and Gas Industry Standard (SY/T5163-2010). TOC analysis was conducted in PetroChina Research Institute of Petroleum Exploration and Development using a Leco CS-230 analyzer referring to the Chinese National Standard (GB/T476-2008). Vitrinite reflectance measurement was conducted by an AXIO Imager Mlm microphotometer produced by the ZEISS company at the China University of Mining and Technology. Approximately 30 values were measured for each shale sample and then averaged to ensure the accuracy of the experimental results.

FE-SEM imaging of shale samples was conducted using a HITACHI SU8020 field emission scanning electron microscopy. The sample was cut into ~10×10×5 mm blocks, and carbon plating was carried out on the sample surface to improve electrical conductivity. Then, the equipment was repeatedly adjusted to make the images of the microscopic pore-fracture structure of shale clearer and more readable. Low-pressure N_2 adsorption was performed in PetroChina Research Institute of Petroleum Exploration and Development using an automatic specific surface area analyzer developed by Quantachrome company, according to the Chinese National Standard (GB/T19587-2004). The specific surface area, pore size, and pore volume of samples were calculated using the Barrett–Joyner–Halenda (BJH) model (Groen et al., 2003).

Fractal theory and technology of porous media have also been used to characterize the pore-fracture structure of shale samples to describe the connectivity and density of porous media quantitatively. Detailed principles and calculation methods of shale samples were illustrated in Yang et al. (2014) and Cai et al. (2017).

Results and analysis

Mineral and organic composition

According to the XRD results, the mineral composition and clay mineral ratio of the shale samples are listed in Tables 1, 2. The minerals of coal-bearing shales from the Shanxi Formation consist of quartz, clay, feldspar, dolomite, siderite, pyrite, together with a few anatase and calcite (Table 1; Figure 2A). Precisely, the quartz content ranges from 17.6 to 65.1%, averaging 40.6%; the clay content ranges from 23.4 to 62%, averaging 45%. The feldspar content varies from 0.4 to 2.8%, with a mean value of 2.8%; the siderite content has an average value of 1.5%. Calcite and dolomite occur only in a few shale samples and are present in very low concentrations. Pyrite is developed in most shale samples with an average of 5.2%, and anatase also appears in some samples with a low average content of 1.0% (Table 2; Figure 2A). As for the clay minerals, the mixed-layer illite-smectite (I/S) content range from 16 to 59%, averaging 31.6%, and the illite content varies from 15 to 35.6%, with a mean value of 25.4%. Kaolinite content ranges from 3.7 to 50% averaging 38.3%, and smectite content varies from 1.7 to 8.0%, having a mean value of 4.7% (Figure 2B).

TOC content of shale samples ranges from 0.1 to 36.7%, with an average of 8.1% (Figure 3). The TOC results suggest that the studied shale belongs to organic-rich shale (TOC > 2.0%). Ro values of some shale samples vary from 2.32 to 2.48% averaging 2.41%, indicating coal-bearing shale has reached the stage of dry gas generation with a potential for hydrocarbon generation.

Pore type and morphology

The typical N_2 adsorption-desorption curves of the studied samples are shown in Figure 4, and the isothermal curves are similar to the inverse "S" shape. These representative curves show that different samples developed different pore types, which resulted in a diverse variation trend of the curves. When the relative pressure is high, the isothermal adsorption curve rises rapidly, showing a downward concave trend, and the adsorption and desorption process has irreversibility. Subsequently, the adsorption and desorption curves are separated to form hysteresis loops (Bu et al., 2015; Yu et al., 2020). Based on the classification of Sing and Williams (2004), the adsorption-desorption curves of shale samples in the study area can be roughly divided into two types, namely, type B and type C. Type B refers to an adsorption-desorption curve with an obvious hysteresis loop (Figure 4C). Type C is the adsorption curve and desorption curve approximately consistent, and a slight hysteresis loop exists (Figures 4A,B,D). Generally, the shape of the hysteresis loop can be applied to interpret the morphology of pores in shale samples (Clarkson et al., 2012b; Yang et al., 2021). The shape of the hysteresis loop is relatively wide, indicating that the pore type is mainly the shape of a thin neck and wide-body inkbottle (such as SY1). While the shape of the hysteresis loop is not obvious, indicating that the pore type is mainly cylindrical pore or parallel plate (such as SY5).

SEM images show that the pores in coal-bearing shale can be divided into three types: intergranular pores, intragranular pores and organic pores (Loucks et al., 2012). Organic pores are generally round or oval, distributed independently in shale matrix, and have relatively poor connectivity (Zeng et al., 2022; Figure 5A). Intergranular pores and intragranular pores are commonly developed in clay minerals, and pores are generally irregular and narrow in shape (Figures 5B–E). Some pores and fractures in clay minerals form several microchannels in the shale matrix

TABLE 2 Clay mineral composition, pore parameters, and Ro values of shale samples.

Samples	I/S (%)	Illite (%)	Kaolinite (%)	Smectite (%)	I/S ratio	Surface area (m^2/g)	Pore volume (cm^3/g)	Average pore size (nm)	Ro (%)
SY1	39.3	30.1	26.3	4.3	16	11.5	0.037	12.9	
SY2	36.0	19.0	37.0	8.0	10	6.636	0.005	1.173	2.48
SY3	35.0	23.0	37.0	5.0	10	8.517	0.006	1.167	
SY4	59.0	35.6	3.7	1.7	12	6.66	0.02	12.14	
SY5	16.0	30.0	50.0	4.0	12	4.639	0.003	0.818	2.32
SY6	31.6	26.6	37.0	4.7	11	9.524	0.03	12.76	
SY7	28.0	20.0	49.0	3.0	14	8.731	0.007	1.155	
SY8	18.0	27.0	50.0	5.0	11	7.511	0.006	1.17	2.44
SY9	21.0	28.0	45.0	6.0	8	0.294	0.001	3.487	
SY10	32.0	15.0	48.0	5.0	9	0.587	0.002	1.024	

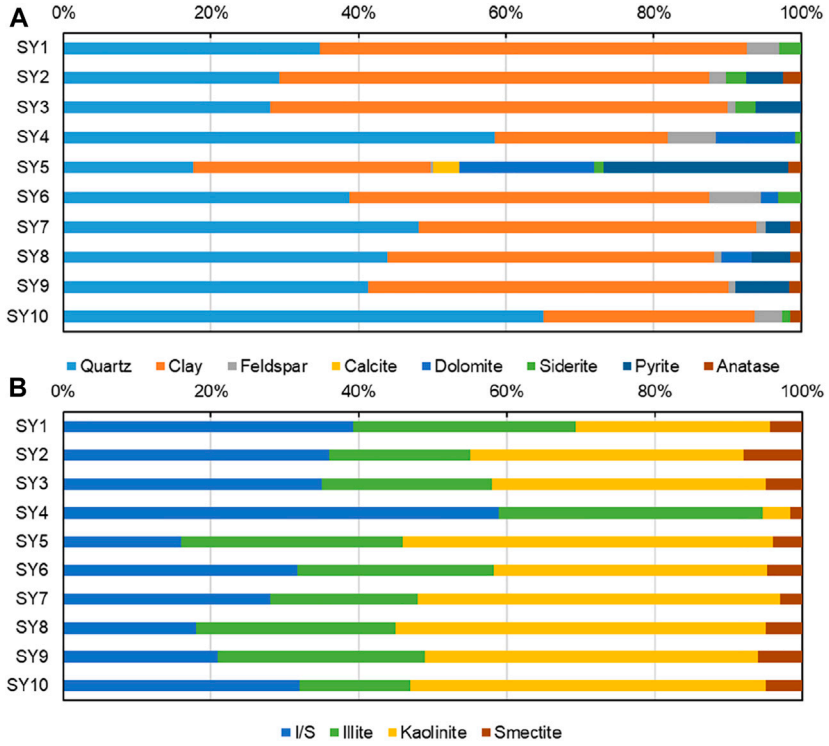

FIGURE 2
Major mineral **(A)** and clay mineral **(B)** composition of shale samples.

with good connectivity (Figures 5B,D). Organic pores are formed by hydrocarbon generation and expulsion of organic matter under a proper temperature and pressure environment. Besides, we also found that a large number of microscopic fractures developed in the shale matrix. On the whole, the connectivity between fractures is poor, and some fractures are filled with clay minerals. The shape of some fractures is arc or root, which indicates that they are affected by tectonic stress to a certain extent (Figures 5B,F). Microfractures in shale are mainly caused by matrix

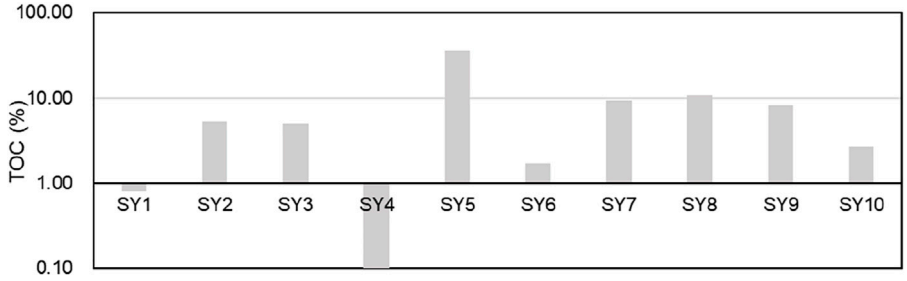

FIGURE 3
TOC content of shale samples.

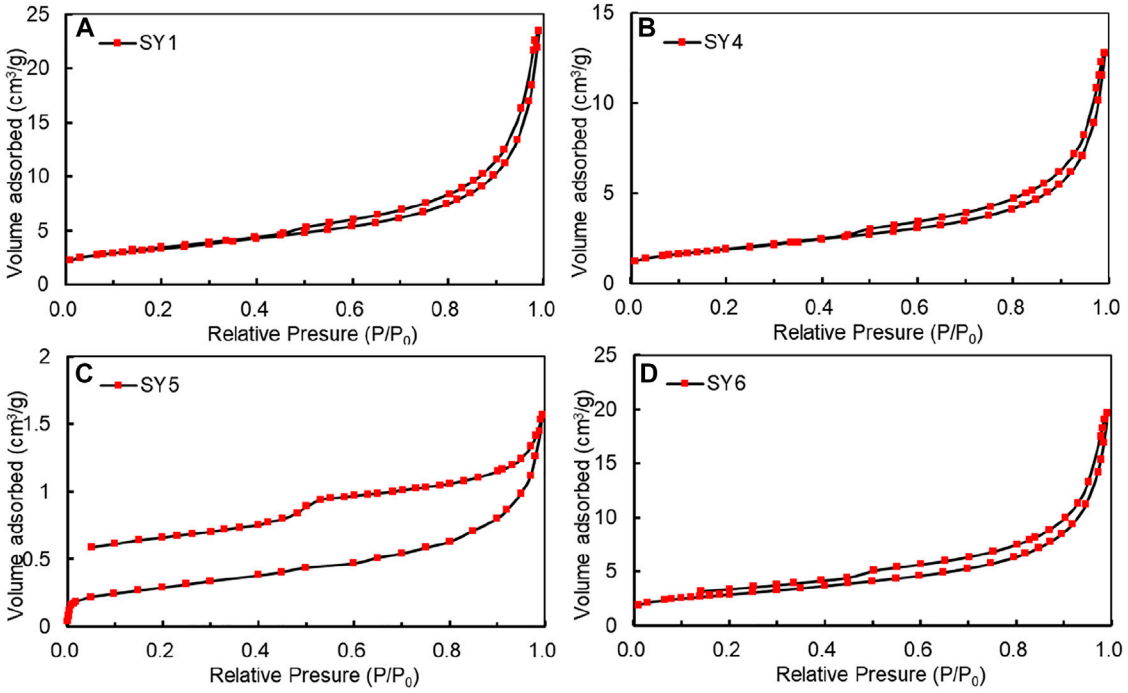

FIGURE 4
Typical low-temperature N_2 adsorption-desorption curves of the studied shale samples.

shrinkage during diagenesis or tectonic compression stress in the later stage. Meanwhile, some regular octahedral pyrite particles are enriched in the shale matrix, confirmed by the pyrite content in the whole rock component (Figure 5E).

Pore size distribution

Based on the N_2 adsorption, the curves of incremental pore volume versus pore size from the typical shale samples are presented in Figure 6. The pore volume and average pore size of the studied shale samples ranged from 0.001 cm^3/g to 0.037 cm^3/g and from 0.82 nm to 12.76 nm, averaging 0.012 cm^3/g 4.78 nm, respectively (Table 2). Within the effective pore size characterized by N_2 adsorption (1–100 nm), the curves of pore size distribution are mostly multi-peak distribution but also appear single-peak distribution. The pore volume of most samples increased sharply in the range of 10–100 nm, and the variation curve of the pore volume of a few samples was not obvious (Figures 6A–D). The pore surface area of samples varies from 0.294 m^2/g to 11.5 m^2/g, with a mean value of 6.46 m^2/g (Table 2). The curves of pore surface area

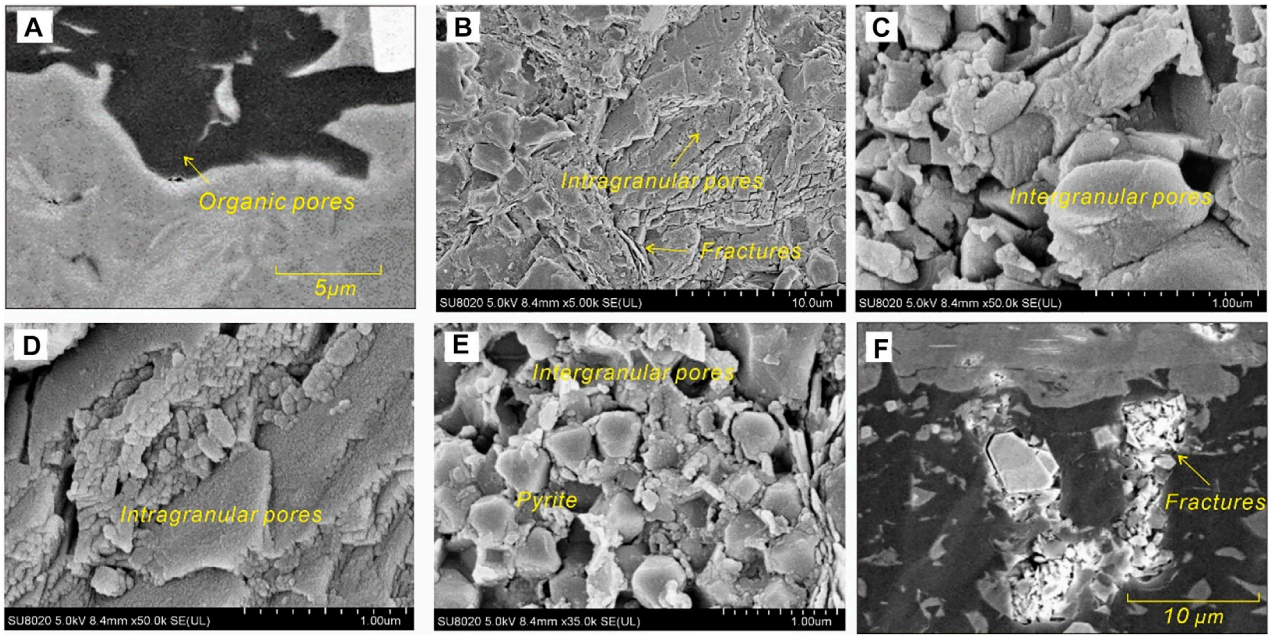

FIGURE 5
Microstructure images of coal-bearing shale in the eastern Ordos Basin, **(A)** Organic pores, **(B)** pore-fracture system in shale matrix, **(C,D)** pores in clay minerals, **(E)** intergranular pores of pyrite, **(F)** fractures in shale matrix.

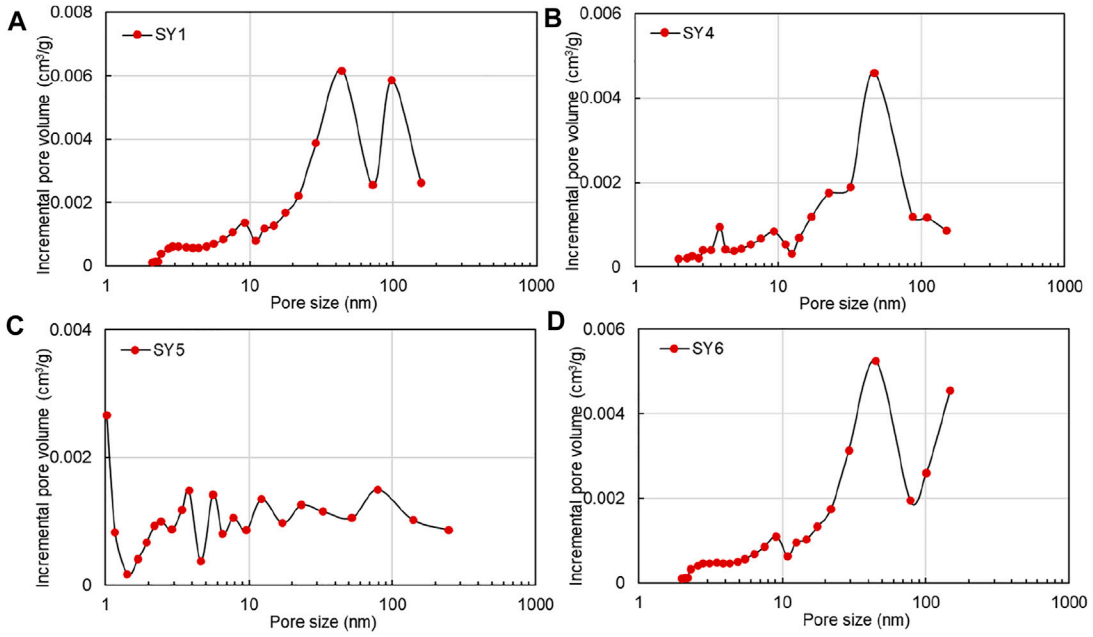

FIGURE 6
Incremental pore volume versus pore size of typical shale samples.

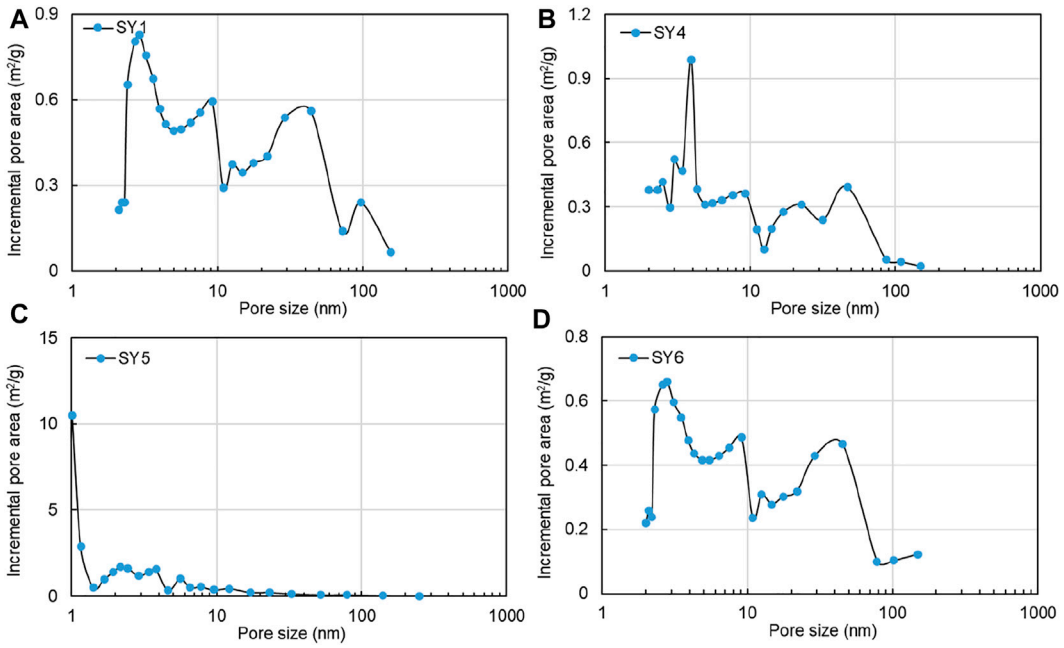

FIGURE 7
Incremental pore area versus pore size of typical shale samples.

versus pore size show that the increment of specific surface area decreases with the increase of pore size. The pore surface area increment is the largest in the range of 1–10 nm, indicating that the smaller the pore size is, the larger the specific surface area is. Meanwhile, the peak value of the increment of pore surface area is also concentrated in the range of 1–10 nm (Figure 7). According to pore surface area and volume distribution curves, pores in shale represented by SY5 are mainly pores with a pore size less than 10 nm, while pores in shale defined by SY1 are mainly pore with pore size between 10–100 nm.

Fractal analysis

In this work, based on the fractal theory (FHH model), we used the equation described to calculate shale fractal dimensions. The linear fitting coefficients (R^2) of all shale samples are greater than 0.95, indicating that the studied samples possess fractal characteristics (Table 3; Figure 8). Besides, all detailed linear equations and fractal dimensions of the studied samples are listed in Table 3. Generally, the values of fractal dimension D range from 2 to 3, and D values are affected by the geometric irregularity and roughness of the surface. The fractal dimensions of the first part (D1) vary from 2.0524 to 2.6325, averaging 2.3641, and that of the second part (D2) range from 2.4061 to 2.8177 with a mean value of 2.7006. These results indicate that the pore structure of the studied shales is complex with strong heterogeneity. More importantly, the larger the D1 value is, the more irregular and rougher the pore surface is. The larger the D2 value is, the more complex the pore structure is (Yang et al., 2017).

Discussion

Influence of mineral and organic composition on pore structure

Organic matter content and mineral composition in shale are the key factors affecting pore structure and distribution in shale matrix. The relationships between pore structure and shale composition are presented in Figure 9. Clay mineral contents show a good correlation with pore specific surface area, especially kaolinite and I/S contents (Figures 9A,B). Kaolinite is positively correlated with specific surface area (R^2=0.5433), while I/S is negatively correlated with specific surface area (R^2=0.6318). Kaolinite derived from feldspar usually occurs in coal-bearing shales as layered aggregates, with many nanopores developed between the layers, increasing specific surface area. I/S usually present a folded section with few nanopores, and its spatial pore structure is affected by the I/S ratio. As for the pore volume, TOC and quartz contents present a positive relationship with pore volume, and no correlation exists between clay content and pore volume (Figures 9C,D). In the high-maturity shales, the

TABLE 3 Fitting equation and fractal dimensions of shale samples.

Samples	Eq. 2	R^2	D2	Eq. 1	R^2	D1
SY1	y = −0.3968x + 1.4207	0.9988	2.6032	y = −0.3675x + 1.3742	0.9988	2.6325
SY2	y = −0.184x + 0.3213	0.993	2.8160	y = −0.7051x + 0.2444	0.9589	2.2949
SY3	y = −0.1823x + 0.5189	0.9839	2.8177	y = −0.8268x + 0.487	0.9601	2.1732
SY4	y = −0.3773x + 0.8548	0.9984	2.6227	y = −0.4093x + 0.8178	0.9998	2.5907
SY5	y = −0.2899x - 0.9166	0.9895	2.7101	y = −0.506x - 0.9838	0.9922	2.494
SY6	y = −0.3758x + 1.2817	0.9976	2.6242	y = −0.3866x + 1.2452	0.9998	2.6134
SY7	y = −0.1986x + 0.6326	0.9895	2.8014	y = −0.6892x + 0.5816	0.9791	2.3108
SY8	y = −0.1942x + 0.3574	0.9856	2.8058	y = −0.6767x + 0.2953	0.97	2.3233
SY9	y = −0.2011x + 0.3265	0.9698	2.7989	y = −0.8441x + 0.3635	0.9944	2.1559
SY10	y = −0.5939x - 2.9052	0.9773	2.4061	y = −0.9476x - 2.8117	0.9521	2.0524

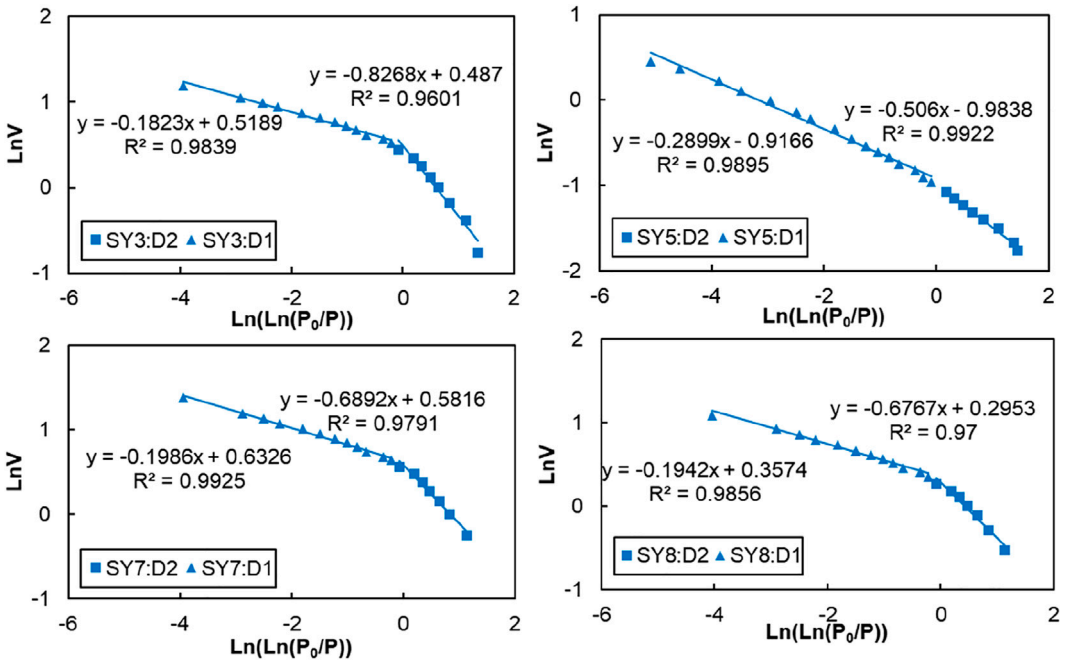

FIGURE 8
Fractal results calculated by N_2 adsorption of typical shale samples.

molecular structure of organic matter is pyrolyzed to generate methane. Gases escape from the surface of organic components, producing a large number of gas pores. The increase of quartz content may lead to brittle fracture of shale and an increase in pore volume. I/S content shows a positive relationship with average pore size, while kaolinite negatively correlates with the average pore size (Figures 9E,F). These relationships suggest that kaolinite is conducive to developing small pores, while more large pores exist in I/S. This understanding is consistent with the correlation between clay minerals and specific surface area.

Relationship between shale brittleness and pore structure

The brittleness of shale determines the development of natural fractures and the formation of a complex network, probably related to pore structure parameters. Shale brittleness was calculated by the following equation described in Rybacki et al. (2016).

$$BRIT = \frac{V_{quartz}}{V_{quartz} + V_{Calcite} + V_{Clay}} \times 100\% \quad (1)$$

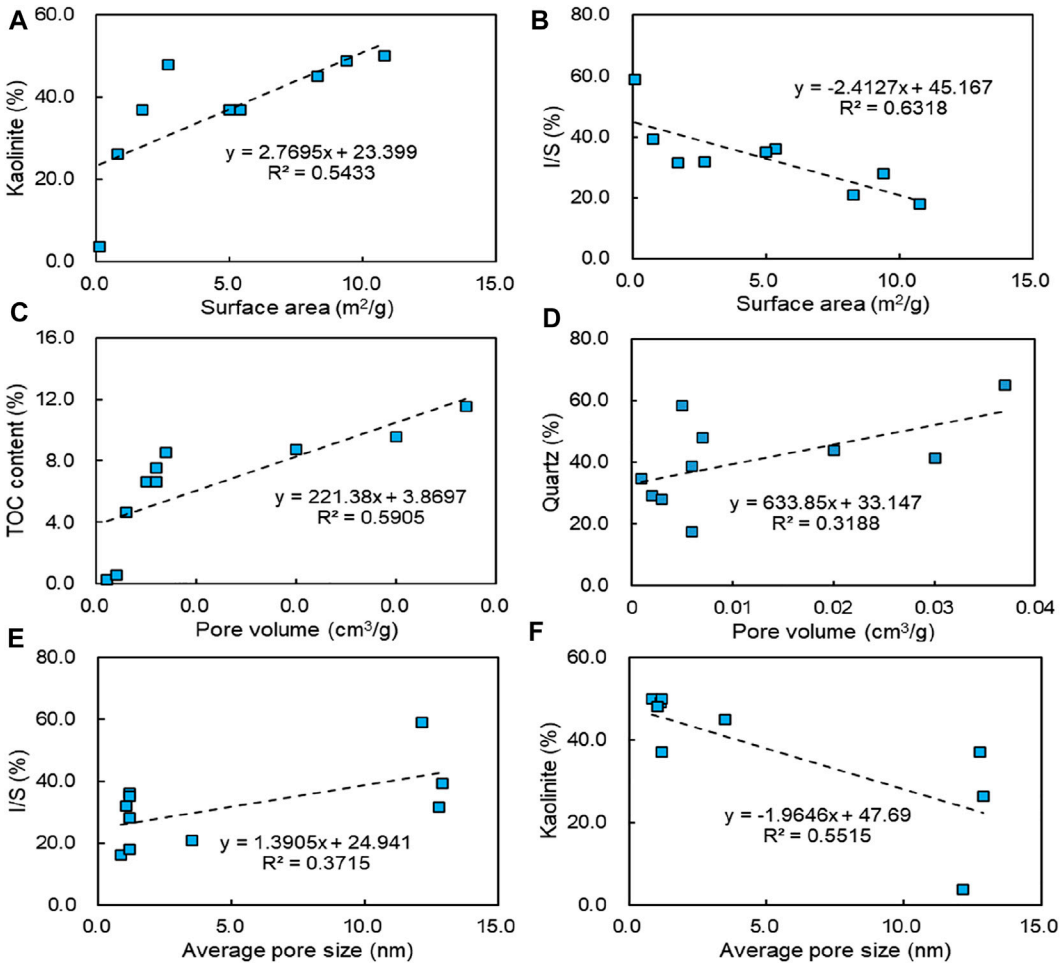

FIGURE 9
Pore structure parameters versus shale composition.

Where V stands for mineral mass fraction, BRIT stands for brittleness index of shale.

The brittleness indexes of all samples ranged from 31.1 to 71.5%, with a mean value of 46.7%. The average brittleness index is higher than 45%, indicating that the reservoir has a certain potential for fracturing and reconstruction. In this study, shale brittleness shows a positive relationship with specific surface area (Figure 10A), indicating the more brittle the shale is, the more microcracks are likely to develop in the matrix thus increasing the specific surface area of the pores. Similarly, there is a positive correlation between brittleness and pore volume (Figure 10B). This trend indicates that fracture channels are commonly developed in shale with high brittleness, increasing pore volume. However, no correlation between shale brittleness and average pore size suggests that shale brittleness has no direct effect on pore size distribution in the studied samples (Figure 10C).

Effect of shale composition and brittleness on fractal dimension

To reveal the influence of shale composition on the fractal dimension, the relationship between fractal dimension and organic matter and mineral contents is shown in Figure 11. Due to the abnormally high TOC value in the SY5 sample, this point was removed for correlation analysis in this study. TOC content positively correlated with D2 characterizing the pore structure complexity, and has a negative relationship with D1 representing the pore surface irregularity (Figures 11A,B), suggesting the increase of organic matter content results in a more complex pore structure and more regular surface. Additionally, quartz and feldspar contents negatively correlate with D2 values, and no relationship exists between quartz, feldspar, and D1 values (Figures 11C,D). These relationships suggest that the increase of homogeneous

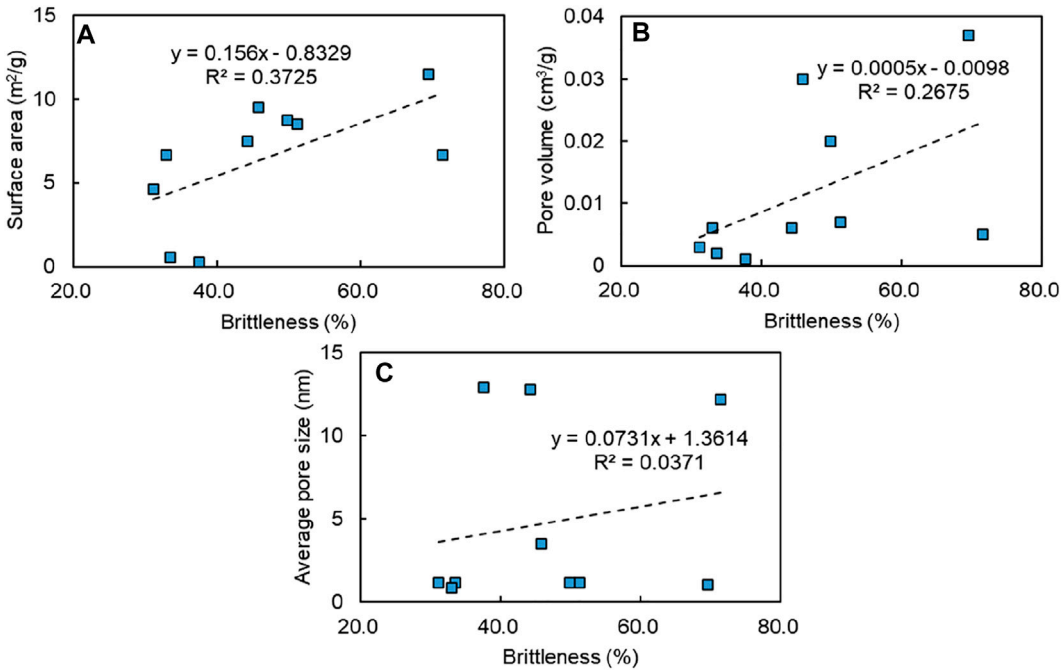

FIGURE 10
Pore structure parameters versus brittleness index in shale.

minerals such as quartz and feldspar probably play a pore-blocking role in the pore system and reduces the shale pore structure's complexity. However, clay minerals possess a positive relationship with D2 values and no obvious correlation with D1 values (Figures 11E,F). This suggests that clay minerals have a more complex structure and thereby increase the heterogeneity and complexity of shale pore structure. Besides, the brittleness indexes exhibit a negative correlation with D2 values, indicating that brittle shales produce more natural microfractures and have a more effective pore system. This relationship increases the spatial connectivity of the pore structure, which in turn naturally decreases D2 values. Overall, the more developed the microscopic pore-fracture system for porous shale, the more homogeneous the reservoir. However, the blocking effect of minerals in the pore-fracture system will reduce the connectivity of the reservoir, which will complicate the fractal dimension of the pore structure.

Heterogeneity of shale microstructure and its implication for methane storage

For understanding the heterogeneity of shale microstructure, the relationship between fractal dimension and pore structure parameters of coal-bearing shale samples is presented in Figure 12. The average pore size shows a negative association with D1 values (Figure 12A), suggesting the mesopore has a rougher and more irregular pore surface than the micropore. This fact is because micropores are round or oval pores formed by hydrocarbon generation, while mesopores are intergranular and intragranular pores of minerals. However, a negative correlation exists between average pore size and D2 values (removed outlier, Figure 12B), indicating that the complexity of shale microstructure may lead to the formation of more micropores, resulting in a decrease in the average pore size. Besides, a negative correlation occurs between pore volume and D1 values, suggesting the more irregular the shale surface, the more pores with small size develop, thus reducing the total pore volume of shale (Figure 12C). There was no obvious correlation between the D2 values and the pore volume, indicating that the complexity of shale pore structure is not necessarily related to pore volume (Figure 12D). It is worth noting that there is no significant correlation between specific surface area and fractal dimensions in this study, which is likely limited by the number and nature of shale samples.

On the other hand, the D1 values on behalf of the pore surface of coal-bearing shale (averaging 2.36) are lower than that

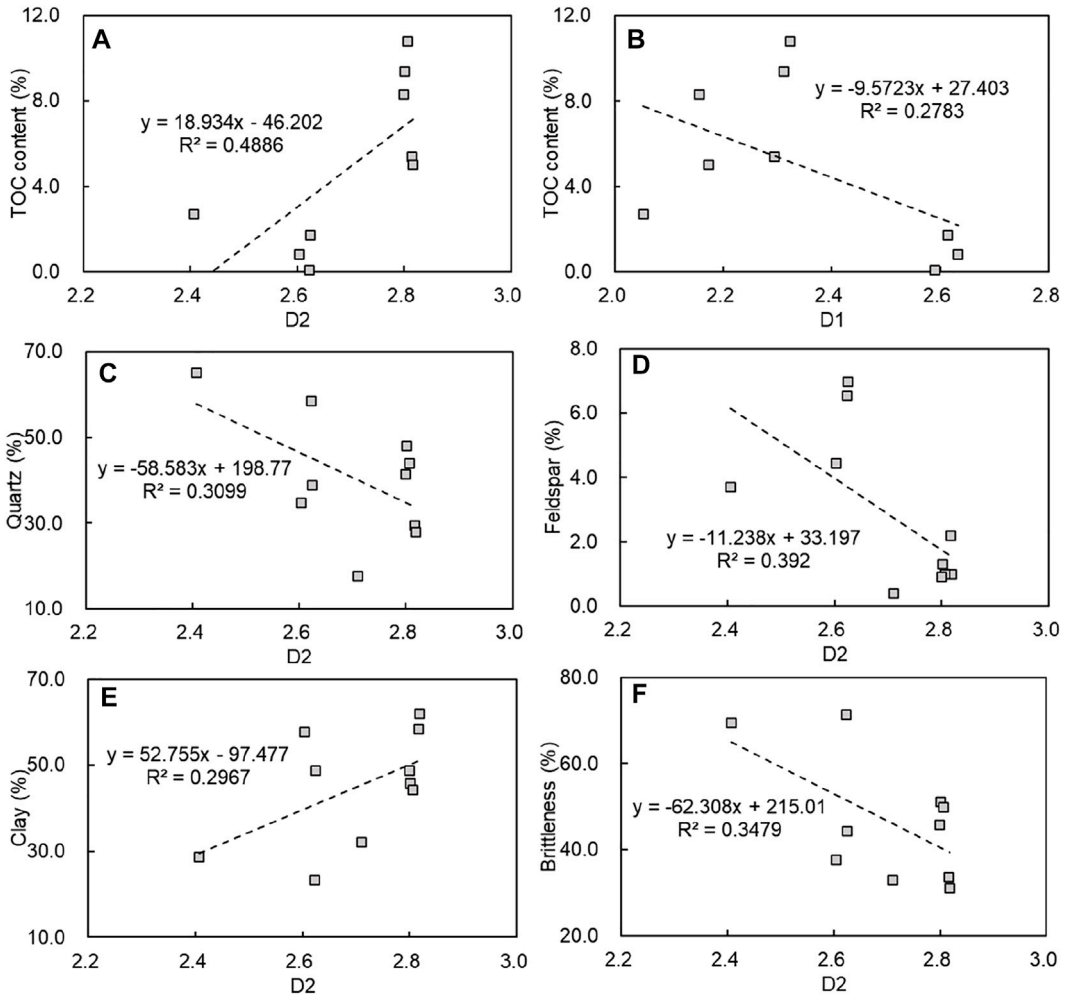

FIGURE 11
Relationship between shale composition, brittleness and fractal dimension.

of marine shale from South China (Longmaxi shale with a mean value of 2.79, Yang et al., 2016). This fact shows that the pores of marine shale with high maturity have more irregular surfaces than coal-bearing shale. Organic pores are developed in marine shale with high maturity, and the surface of organic pores is rougher than that of clay-hosted pores. Additionally, the marine shale has an average D2 value of 2.57 (Liang et al., 2015; Zhang et al., 2017), and the average D2 value of coal-bearing shales is 2.70. Similar D2 values indicate that the pore structures of marine shale and coal-bearing shale are equally complex. In nature, due to the intense hydrocarbon generation of marine shale in South China, many organic pores are generated, which is enhanced the complexity of pore structure. However, the coal-bearing shales in North China have high clay content and numerous clay-hosted pores, making up for the lack of organic pores and presenting a high D2 value. As for the shale gas storage, organic and clay-hosted pores in coal-bearing shale with high maturity may be the main storage space for methane, while the methane is mainly stored in organic pores in marine shale.

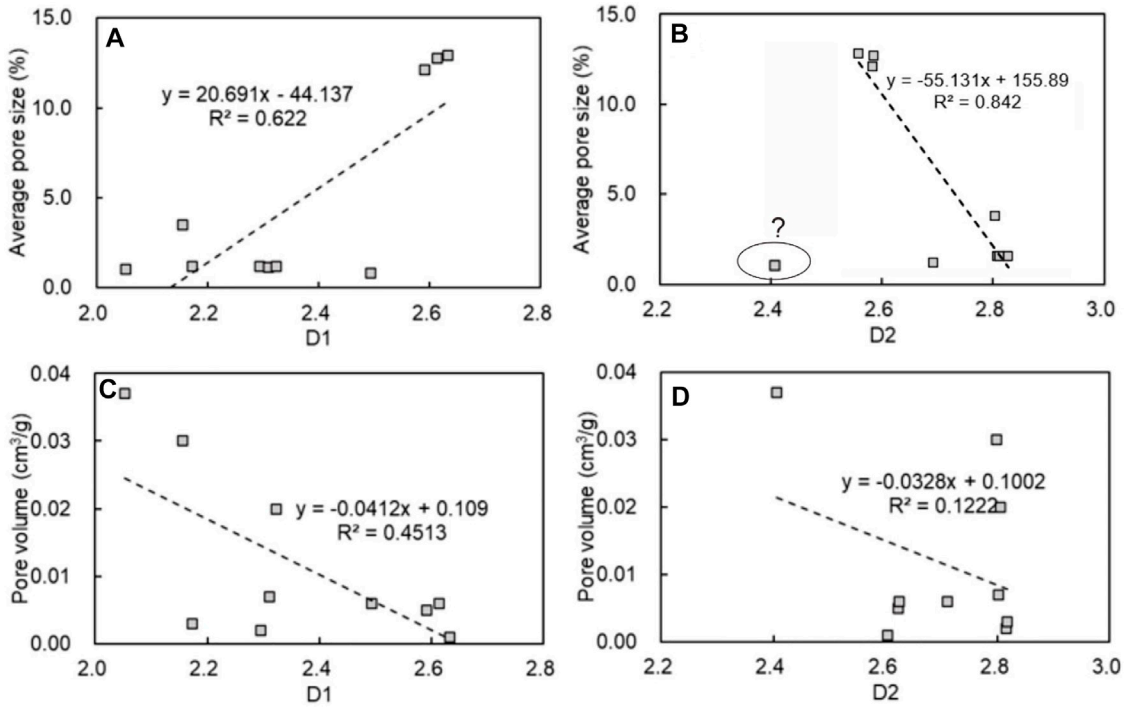

FIGURE 12
Relationship between pore structure and fractal dimension of shale samples.

Conclusion

(a) Kaolinite positively correlates with pore surface area, suggesting that many nanopores formed between the layers result in an increase in specific surface area. The positive relationship between organic matter and pore volume indicates that hydrocarbon generation promotes the formation of gas pores and increases pore volume.

(b) Coal-bearing shales with a high brittleness are probably rich in natural microfractures, which contribute to the increase of specific surface area and pore volume. However, no obvious relationship exists between average pore size and brittleness index.

(c) The more developed the pore-fracture system for porous shale, the more homogeneous the reservoir is. However, the blocking effect of minerals in the pore-fracture system decreases pore connectivity, complicating pore arrangement and enhancing shale heterogeneity.

(d) The pore volume and specific surface area of coal-bearing shale are closely related to the fractal dimensions. The high complexity of the shale microstructure may lead to the formation of more micropores, resulting in a decrease in the average pore size.

(e) By comparing the pore fractal characteristics of marine and coal-bearing shales, organic and clay-hosted pores in coal-bearing shale with high maturity may be the main storage space for methane. In contrast, methane is mainly stored in organic pores in marine shale.

Data availability statement

The datasets presented in this study can be found in online repositories. The names of the repository/repositories and accession number(s) can be found in the article/Supplementary Material.

Author contributions

Investigation, RY, and ZW; methodology, YZ, CL, and WZ; review and editing ZW; data curation, MT, and QC; writing original draft, RY.

Funding

This study was funded by the National Natural Science Foundation of China (No. 41772129).

Acknowledgments

This work was supported by the PetroChina Research Institute of Petroleum Exploration and Development. The authors thank PetroChina Research Institute of Petroleum Exploration and Development for their help and guidance in sample collection, experimental testing and data analysis.

Conflict of interest

Author CL is employed by the CNOOC Energy Development Co., LTD.

The remaining authors declare that the research was conducted in the absence of any commercial or financial relationships that could be construed as a potential conflict of interest.

Publisher's note

References

Arif, M., Mahmoud, M., Zhang, Y., and Iglauer, S. (2021). X-Ray tomography imaging of shale microstructures: A review in the context of multiscale correlative imaging. *Int. J. Coal Geol.* 233, 103641. doi:10.1016/j.coal.2020.103641

Bowker, K. A. (2007). Barnett shale gas production, fort worth basin: Issues and discussion. *Am. Assoc. Pet. Geol. Bull.* 91 (4), 523–533. doi:10.1306/06190606018

Bu, H., Ju, Y., Tan, J., Wang, G., and Li, X. (2015). Fractal characteristics of pores in non-marine shales from the Huainan coalfield, eastern China. *J. Nat. Gas Sci. Eng.* 24, 166–177. doi:10.1016/j.jngse.2015.03.021

Cai, J., Wei, W. E. I., Hu, X., Liu, R., and Wang, J. (2017). Fractal characterization of dynamic fracture network extension in porous media. *Fractals* 25 (02), 1750023. doi:10.1142/s0218348x17500232

Clarkson, C. R., Jensen, J. L., Pedersen, P. K., and Freeman, M. (2012a). Innovative methods for flow-unit and pore-structure analyses in a tight siltstone and shale gas reservoir. *Am. Assoc. Pet. Geol. Bull.* 96 (2), 355–374. doi:10.1306/05181110171

Clarkson, C. R., Nobakht, M., Kaviani, D., and Ertekin, T. (2012b). Production analysis of tight-gas and shale-gas reservoirs using the dynamic-slippage concept. *SPE J.* 17 (01), 230–242. doi:10.2118/144317-pa

Curtis, M. E., Cardott, B. J., Sondergeld, C. H., and Rai, C. S. (2012). Development of organic porosity in the Woodford Shale with increasing thermal maturity. *Int. J. Coal Geol.* 103, 26–31. doi:10.1016/j.coal.2012.08.004

Dai, S., Ren, D., Chou, C. L., Finkelman, R. B., Seredin, V. V., and Zhou, Y. (2012). Geochemistry of trace elements in Chinese coals: A review of abundances, genetic types, impacts on human health, and industrial utilization. *Int. J. Coal Geol.* 94, 3–21. doi:10.1016/j.coal.2011.02.003

Gao, Z., Fan, Y., Xuan, Q., and Zheng, G. (2020). A review of shale pore structure evolution characteristics with increasing thermal maturities. *Adv. Geo-Energy Res.* 4 (3), 247–259. doi:10.46690/ager.2020.03.03

Garum, M., Glover, P. W., Lorinczi, P., Drummond-Brydson, R., and Hassanpour, A. (2020). Micro-and nanoscale pore structure in gas shale using Xμ-CT and FIB-SEM techniques. *Energy fuels.* 34 (10), 12340–12353. doi:10.1021/acs.energyfuels.0c02025

Groen, J. C., Peffer, L. A., and Pérez-Ramı´rez, J. (2003). Pore size determination in modified micro-and mesoporous materials. Pitfalls and limitations in gas adsorption data analysis. *Microporous mesoporous Mater.* 60 (1-3), 1–17. doi:10.1016/s1387-1811(03)00339-1

Hamawand, I., Yusaf, T., and Hamawand, S. G. (2013). Coal seam gas and associated water: A review paper. *Renew. Sustain. energy Rev.* 22, 550–560. doi:10.1016/j.rser.2013.02.030

Hao, F., Zou, H., and Lu, Y. (2013). Mechanisms of shale gas storage: Implications for shale gas exploration in China. *Am. Assoc. Pet. Geol. Bull.* 97 (8), 1325–1346. doi:10.1306/02141312091

Heller, R., and Zoback, M. (2014). Adsorption of methane and carbon dioxide on gas shale and pure mineral samples. *J. Unconv. oil gas Resour.* 8, 14–24. doi:10.1016/j.juogr.2014.06.001

Huang, B., Zhao, X., and Zhang, Q. (2016). Framework of the theory and technology for simultaneous mining of coal and its associated resources. *J. China Univ. Min. Technol.* 45 (4), 653–662.

Jarvie, D. M., Hill, R. J., Ruble, T. E., and Pollastro, R. M. (2007). Unconventional shale-gas systems: The Mississippian Barnett Shale of north-central Texas as one model for thermogenic shale-gas assessment. *Am. Assoc. Pet. Geol. Bull.* 91 (4), 475–499. doi:10.1306/12190606068

Ju, Y., Yu, K., Wang, G., Li, W., Zhang, K., Li, S., et al. (2021). Coupling response of the Meso–Cenozoic differential evolution of the North China Craton to lithospheric structural transformation. *Earth-Science Rev.* 223, 103859. doi:10.1016/j.earscirev.2021.103859

Klaver, J., Desbois, G., Littke, R., and Urai, J. L. (2015). BIB-SEM characterization of pore space morphology and distribution in postmature to overmature samples from the Haynesville and Bossier Shales. *Mar. Petroleum Geol.* 59, 451–466. doi:10.1016/j.marpetgeo.2014.09.020

Kuila, U., McCarty, D. K., Derkowski, A., Fischer, T. B., Topór, T., and Prasad, M. (2014). Nanoscale texture and porosity of organic matter and clay minerals in organic-rich mudrocks. *Fuel* 135, 359–373. doi:10.1016/j.fuel.2014.06.036

Li, J., Yin, J., Zhang, Y., Lu, S., Wang, W., Li, J., et al. (2015). A comparison of experimental methods for describing shale pore features—A case study in the bohai bay basin of eastern China. *Int. J. Coal Geol.* 152, 39–49. doi:10.1016/j.coal.2015.10.009

Li, Y., Pan, S., Ning, S., Shao, L., Jing, Z., and Wang, Z. (2022a). Coal measure metallogeny: Metallogenic system and implication for resource and environment. *Sci. China Earth Sci.* 65, 1211–1228. doi:10.1007/s11430-021-9920-4

Li, Y., Chen, J., Elsworth, D., Pan, Z., and Ma, X. (2022b). Nanoscale mechanical property variations concerning mineral composition and contact of marine shale. *Geosci. Front.* 13. doi:10.1016/j.gsf.2022.101405

Liang, L., Xiong, J., and Liu, X. (2015). An investigation of the fractal characteristics of the Upper Ordovician Wufeng Formation shale using nitrogen adsorption analysis. *J. Nat. Gas Sci. Eng.* 27, 402–409. doi:10.1016/j.jngse.2015.07.023

Liu, Y., Yao, Y., Liu, D., Zheng, S., Sun, G., and Chang, Y. (2018). Shale pore size classification: An NMR fluid typing method. *Mar. Petroleum Geol.* 96, 591–601. doi:10.1016/j.marpetgeo.2018.05.014

Loucks, R. G., Reed, R. M., Ruppel, S. C., and Jarvie, D. M. (2009). Morphology, Genesis, and distribution of nanometer-scale pores in siliceous mudstones of the Mississippian Barnett Shale. *J. Sediment. Res.* 79 (12), 848–861. doi:10.2110/jsr.2009.092

Loucks, R. G., Reed, R. M., Ruppel, S. C., and Hammes, U. (2012). Spectrum of pore types and networks in mudrocks and a descriptive classification for matrix-related mudrock pores. *Am. Assoc. Pet. Geol. Bull.* 96 (6), 1071–1098. doi:10.1306/08171111061

McGlade, C., Speirs, J., and Sorrell, S. (2013). Methods of estimating shale gas resources–Comparison, evaluation and implications. *Energy* 59, 116–125. doi:10.1016/j.energy.2013.05.031

Pan, J., Peng, C., Wan, X., Zheng, D., Lv, R., and Wang, K. (2017). Pore structure characteristics of coal-bearing organic shale in Yuzhou coalfield, China using low pressure N2 adsorption and FESEM methods. *J. Petroleum Sci. Eng.* 153, 234–243. doi:10.1016/j.petrol.2017.03.043

Ross, D. J., and Bustin, R. M. (2009). The importance of shale composition and pore structure upon gas storage potential of shale gas reservoirs. *Mar. Petroleum Geol.* 26 (6), 916–927. doi:10.1016/j.marpetgeo.2008.06.004

Rybacki, E., Meier, T., and Dresen, G. (2016). What controls the mechanical properties of shale rocks?–Part II: Brittleness. *J. Petroleum Sci. Eng.* 144, 39–58. doi:10.1016/j.petrol.2016.02.022

Saif, T., Lin, Q., Bijeljic, B., and Blunt, M. J. (2017). Microstructural imaging and characterization of oil shale before and after pyrolysis. *Fuel* 197, 562–574. doi:10.1016/j.fuel.2017.02.030

Shan, C., Zhang, T., Guo, J., Zhang, Z., and Yang, Y. (2015). Characterization of the micropore systems in the high-rank coal reservoirs of the southern Sichuan Basin, China. *Am. Assoc. Pet. Geol. Bull.* 99 (11), 2099–2119. doi:10.1306/07061514240

Sing, K. S., and Williams, R. T. (2004). Physisorption hysteresis loops and the characterization of nanoporous materials. *Adsorpt. Sci. Technol.* 22 (10), 773–782. doi:10.1260/0263617053499032

Tang, X., Jiang, Z., Li, Z., Gao, Z., Bai, Y., Zhao, S., et al. (2015). The effect of the variation in material composition on the heterogeneous pore structure of high-maturity shale of the Silurian Longmaxi formation in the southeastern Sichuan Basin, China. *J. Nat. Gas Sci. Eng.* 23, 464–473. doi:10.1016/j.jngse.2015.02.031

Uysal, I. T., Golding, S. D., and Glikson, M. (2000). Petrographic and isotope constraints on the origin of authigenic carbonate minerals and the associated fluid evolution in Late Permian coal measures, Bowen Basin (Queensland), Australia. *Sediment. Geol.* 136 (3-4), 189–206. doi:10.1016/s0037-0738(00)00097-x

Valenza, J. J., Drenzek, N., Marques, F., Pagels, M., and Mastalerz, M. (2013). Geochemical controls on shale microstructure. *Geology* 41 (5), 611–614. doi:10.1130/g33639.1

Wang, X., Tang, Y., Wang, S., and Schobert, H. H. (2020). Clean coal geology in China: Research advance and its future. *Int. J. Coal Sci. Technol.* 7 (2), 299–310. doi:10.1007/s40789-020-00321-4

Yang, F., Ning, Z., and Liu, H. (2014). Fractal characteristics of shales from a shale gas reservoir in the Sichuan Basin, China. *Fuel* 115, 378–384. doi:10.1016/j.fuel.2013.07.040

Yang, R., He, S., Yi, J., and Hu, Q. (2016). Nanoscale pore structure and fractal dimension of organic-rich Wufeng-Longmaxi shale from Jiaoshiba area, Sichuan Basin: Investigations using FE-SEM, gas adsorption and helium pycnometry. *Mar. Petroleum Geol.* 70, 27–45. doi:10.1016/j.marpetgeo.2015.11.019

Yang, J., Hatcherian, J., Hackley, P. C., and Pomerantz, A. E. (2017). Nanoscale geochemical and geomechanical characterization of organic matter in shale. *Nat. Commun.* 8 (1), 2179–9. doi:10.1038/s41467-017-02254-0

Yang, W., Song, Y., Jiang, Z., Luo, Q., Wang, Q., Yuan, Y., et al. (2018). Whole-aperture characteristics and controlling factors of pore structure in the Chang 7th continental shale of the Upper Triassic Yanchang Formation in the southeastern Ordos Basin, China. *Interpretation* 6 (1), T175–T190. doi:10.1190/int-2017-0090.1

Yang, W., Wang, Q., Wang, Y., Jiang, Z., Song, Y., Li, Y., et al. (2020). Pore characteristic responses to categories of depositional microfacies of delta-lacustrine tight reservoirs in the Upper Triassic Yanchang Formation, Ordos Basin, NW China. *Mar. Petroleum Geol.* 118, 104423. doi:10.1016/j.marpetgeo.2020.104423

Yang, W., Xu, L., Chen, D. X., Jiang, Z. X., Zhang, Z. Y., Hao, B., et al. (2021). How argillaceous reservoirs exhibit better quality than silty mudstones? Anomalous behavior of shale gas-bearing properties of continental fine-grained sediments in southwest China and its possible forcing mechanisms. *Petroleum Sci.* 18 (6), 1589–1610. doi:10.1016/j.petsci.2021.09.032

Yu, K., Shao, C., Ju, Y., and Qu, Z. (2019). The Genesis and controlling factors of micropore volume in transitional coal-bearing shale reservoirs under different sedimentary environments. *Mar. Petroleum Geol.* 102, 426–438. doi:10.1016/j.marpetgeo.2019.01.003

Yu, K., Ju, Y., and Shao, C. (2020). Structure characteristics and evolution mechanism of nanopore in transitional coal-bearing shale. *J. Petroleum Sci. Eng.* 184, 106545. doi:10.1016/j.petrol.2019.106545

Yu, K., Ju, Y., Wan, Z., and Zhao, K. (2022). Paleoenvironment, provenance, and hydrocarbon potential of lower permian coal-bearing source rocks in the southern north China basin: A case study of the pingdingshan coalfield. *ACS Earth Space Chem.* 6 (5), 1299–1310. doi:10.1021/acsearthspacechem.2c00003

Zeng, X., Wang, W., Cao, Q., Zhou, S., Dong, G., Wang, A., et al. (2022). *Evaluation of the accumulation conditions and favorable areas of shale gas in the upper palaeozoic marine-continental transitional facies in the daning-jixian area*. Geofluids: Ordos Basin.

Zhang, J., Li, X., Wei, Q., Sun, K., Zhang, G., and Wang, F. (2017). Characterization of full-sized pore structure and fractal characteristics of marine–continental transitional Longtan Formation shale of Sichuan Basin, South China. *Energy fuels.* 31 (10), 10490–10504. doi:10.1021/acs.energyfuels.7b01456

Zhang, Q., Qiu, Z., Zhao, Q., Zhang, L., Dong, D., Wang, Y., et al. (2022). Composition effect on the pore structure of transitional shale: A case study of the permian Shanxi Formation in the daning–jixian block at the eastern margin of the Ordos Basin. *Front. Earth Sci. (Lausanne).* 9, 1407. doi:10.3389/feart.2021.802713

Zhu, H., Ju, Y., Huang, C., Han, K., Qi, Y., Shi, M., et al. (2019). Pore structure variations across structural deformation of silurian longmaxi shale: An example from the chuandong thrust-fold belt. *Fuel* 241, 914–932. doi:10.1016/j.fuel.2018.12.108

Zou, C. N., Yang, Z., Huang, S. P., Ma, F., Sun, Q. P., Li, F. H., et al. (2019). Resource types, formation, distribution and prospects of coal-measure gas. *Petroleum Explor. Dev.* 46 (3), 451–462. doi:10.1016/s1876-3804(19)60026-1